Physica A 389 (2010) 3069–3080

Contents lists available at ScienceDirect

Physica A

journal homepage: www.elsevier.com/locate/physa

Rarefaction effects in thermally-driven microflows

Peyman Taheri *, Henning Struchtrup

Department of Mechanical Engineering, University of Victoria, P.O. Box 3055, STN CSC, Victoria, British Columbia, Canada, V8W 3P6

ARTICLE INFO

Article history:
Received 28 December 2009
Available online 8 April 2010

Keywords:
Kinetic theory of gases
Rarefied gas flow
Thermal creep flow
Thermal transpiration flow
Knudsen boundary layers
Grad's moment method

ABSTRACT

Rarefied gas flow in a parallel-plate micro-channel is considered, where a streamwise constant temperature gradient is applied in the channel walls. An analytical approach to the problem is conducted based on linearized and semi-linearized forms of the regularized 13-moment equations (R13 equations), which are a set of macroscopic transport equations for rarefied gases at the super-Burnett order. Typical nonequilibrium effects at the boundary, i.e., velocity slip, temperature jump, and formation of Knudsen boundary layers are investigated. Nonlinear contributions lead to temperature, density, and normal stress profiles across the channel which are not reported elsewhere in literature.

1. Introduction

Thermal creep flows occur in gases when nonuniform temperature distributions are applied in the flow boundaries [1]. In the case of channel flows, this simple boundary treatment induces a tangential creep velocity in the interior gas close to the walls, such that the gas flows in the direction of the temperature gradient, i.e., from cold to hot. In moderately rarefied gases, this thermally induced velocity initiates within a thin boundary layer. The thickness of this creep layer is proportional to the Knudsen number, *Kn*. In sufficiently long channels, the velocity gradient within the creep layer might fill the whole channel width, as the result of shear stress diffusion. This phenomenon was first reported in 1879 by Reynolds as *thermal transpiration flow* [2]. At the same time, Maxwell was trying to provide a physical explanation for this problem [3]. Later experimental observations by Knudsen proved the existence of a pumping effect in thermal creep (or thermal transpiration) flows; he obtained a ten-fold pressure increase between the inlet and outlet of a series of heated tubes [4,5].

Nowadays, nonuniformly heated channels are used in miniaturized devices as pumps or compressors with no moving parts, so-called Knudsen pumps or compressors, which operate based on thermal creep/transpiration flow [6,7]. Furthermore, thermally-driven and pressure-driven flows may be combined in order to control mass and energy flow rates in micro-channels.

Similar to other nonequilibrium flows, thermal creep/transpiration flow is not amenable to classical hydrodynamics, as described by the Navier–Stokes–Fourier (NSF) equations. Consequently, the problem is investigated by several authors using kinetic models for the Boltzmann equation. The flow between two parallel plates, where a constant unidimensional temperature gradient is applied to the plates, is a common flow configuration which is used in kinetic approaches. Some of the kinetic data for this particular problem are collected, and carefully compared in Ref. [8]. In general, the kinetic data are obtained using either the Bhatnagar–Gross–Krook (BGK) kinetic model for the Boltzmann equation, or the linearized form of the Boltzmann equation itself (LB). The main difference between the BGK and LB kinetic models is that the BGK yields a wrong Prandtl number $Pr^{\mathrm{BGK}} = 1$, while the correct value can be predicted by the LB method, $Pr^{\mathrm{LB}} = 2/3$ (for

* Corresponding author.
E-mail addresses: peymant@uvic.ca (P. Taheri), struchtr@uvic.ca (H. Struchtrup).
URL: http://www.engr.uvic.ca/~struchtr (H. Struchtrup).

0378-4371/$ – see front matter © 2010 Elsevier B.V. All rights reserved.
doi:10.1016/j.physa.2010.03.050

ideal monatomic gases). Kinetic solutions for thermal transpiration flow with the BGK model are reported in Refs. [9–13], using different numerical schemes. Further kinetic data based on a linearized Boltzmann equation (LB) are also available in Refs. [14,15].

Approximation methods in kinetic theory [16] derive macroscopic transport equations from the Boltzmann kinetic equation at different levels of accuracy. Conventionally, these high-order continuum models are derived based on either the Chapman–Enskog expansion method [17] or Grad's moment expansion method [18,19].

Burnett-type equations follow from the Chapman–Enskog expansion in the Knudsen number, where the second- and third-order expansions give Burnett and super-Burnett equations, respectively. It is important to mention that classical Burentt and super-Burnett equations suffer from instabilities [20,21]. Consequently, several techniques are proposed to stabilize these equations including the augmented Burnett equations [22], the regularized Burnett equations [23], consistently ordered extended thermodynamics [24], the hyperbolic Burnett equations [25], and the hybrid Burnett equations [26].

In the present study a macroscopic approach to temperature induced flows in parallel-plate micro-channels is presented. This paper forms a sequel to our previous works [27–29], where an accessible analytical approach successfully describes the interaction between bulk and rarefaction effects in common flow configurations. The regularized 13-moment (R13) equations in their fully linearized and semi-linearized forms are adapted for thermally-driven flows with arbitrary Knudsen numbers. The R13 equations are appropriate for rarefied flows in the transition regime, i.e., $Kn < 1$, and provide a stable set of transport equations [30,16] of the super-Burnett order, $\mathcal{O}(Kn^3)$. In contrast to their classical counterpart, i.e., Grad's 13-moment system [18,19], the R13 equations are able to capture Knudsen boundary layers [31,32]. Thus, they cover the whole spectrum of flow between the linear regime, where effects like Knudsen layers dominate, and the nonlinear regime, where nonlinear bulk effects and shocks [33] become important.

2. Regularized 13-moment equations

The regularized 13-moment equations are based on the conservation laws for mass, momentum, and energy

$$\frac{D\rho}{Dt} + \rho\frac{\partial v_k}{\partial x_k} = 0, \tag{1}$$

$$\rho\frac{Dv_i}{Dt} + \frac{\partial p_{ik}}{\partial x_k} = \rho G_i, \tag{2}$$

$$\rho\frac{De}{Dt} + \frac{\partial\,(p_{ik}v_i + q_k)}{\partial x_k} = \rho G_i v_i, \tag{3}$$

where t, ρ and e stand for time, mass density, and (total) energy density. The vectors x_k, v_k, G_i and q_k represent spatial position, velocity, body force and heat flux. The pressure tensor is $p_{ik} = p\delta_{ik} + \sigma_{ik}$, where δ_{ik} is the Kronecker delta. Pressure $p = p_{kk}/3$, and stress tensor $\sigma_{ik} = p_{\langle ik\rangle}$ are equilibrium and nonequilibrium parts of the pressure tensor, respectively. Since we consider ideal monatomic gases, $p = \rho\theta$ holds as the equation of state, where θ is the temperature in energy units ($\theta = \mathcal{R}T$ where $\mathcal{R}$ is the gas constant and T is thermodynamic temperature). The convective derivative is $D_t = \partial_t + v_k\,\partial_{x_k}$.

The R13 system includes balance equations for heat-flux vector and stress tensor as their respective moment equations

$$\begin{aligned}\frac{Dq_i}{Dt} &+ \underline{\frac{5}{2}p\frac{\partial\theta}{\partial x_i}} + \frac{5}{2}\sigma_{ik}\frac{\partial\theta}{\partial x_k} - \sigma_{ik}\theta\frac{\partial\ln\rho}{\partial x_k} - \frac{\sigma_{ij}}{\rho}\frac{\partial\sigma_{jk}}{\partial x_k} + \theta\frac{\partial\sigma_{ik}}{\partial x_k}\\ &+ \frac{7}{5}q_k\frac{\partial v_i}{\partial x_k} + \frac{7}{5}q_i\frac{\partial v_k}{\partial x_k} + \frac{2}{5}q_k\frac{\partial v_k}{\partial x_i} + \frac{1}{2}\frac{\partial R_{ik}}{\partial x_k} + \frac{1}{6}\frac{\partial\Delta}{\partial x_i} + m_{ijk}\frac{\partial v_j}{\partial x_k} = \underline{-Pr\frac{p}{\mu}}q_i,\end{aligned} \tag{4}$$

and

$$\frac{D\sigma_{ij}}{Dt} + \underline{2p\frac{\partial v_{\langle i}}{\partial x_{j\rangle}}} + \sigma_{ij}\frac{\partial v_k}{\partial x_k} + \frac{4}{5}\frac{\partial q_{\langle i}}{\partial x_{j\rangle}} + 2\sigma_{k\langle i}\frac{\partial v_{j\rangle}}{\partial x_k} + \frac{\partial m_{ijk}}{\partial x_k} = \underline{-\frac{p}{\mu}}\sigma_{ij}, \tag{5}$$

where $Pr = 2/3$ is the Prandtl number for ideal monatomic gases and μ is the gas viscosity. The indices inside angular brackets indicate symmetric trace-free tensors; the trace-free part of the matrix A_{ij} is $A_{\langle ij\rangle} = (A_{ij} + A_{ji})/2 - A_{kk}\,\delta_{ij}/3$, and similarly for three indices, see Ref. [16, pg. 231].

The extended balance equations [cf. Eqs. (4) and (5)] contain the additional higher moments Δ, R_{ij} and m_{ijk}. These higher order moments vanish in Grad's classical 13-moment system [18,19], while the regularization gives

$$\Delta = -\frac{\sigma_{ij}\sigma_{ij}}{\rho} - 12\frac{\mu}{p}\left(\theta\frac{\partial q_k}{\partial x_k} + \frac{5}{2}q_k\frac{\partial\theta}{\partial x_k} - \theta q_k\frac{\partial\ln\rho}{\partial x_k} + \theta\sigma_{kl}\frac{\partial v_k}{\partial x_l}\right), \tag{6}$$

$$R_{ij} = -\frac{4}{7}\frac{\sigma_{k\langle i}\sigma_{j\rangle k}}{\rho} - \frac{24}{5}\frac{\mu}{p}\left(\theta\frac{\partial q_{\langle i}}{\partial x_{j\rangle}} + q_{\langle i}\frac{\partial\theta}{\partial x_{j\rangle}} - \theta q_{\langle i}\frac{\partial\ln\rho}{\partial x_{j\rangle}} + \frac{10}{7}\theta\sigma_{k\langle i}S_{j\rangle k}\right), \tag{7}$$

$$m_{ijk} = -2\frac{\mu}{p}\left(\theta\frac{\partial\sigma_{\langle ij}}{\partial x_{k\rangle}} - \theta\sigma_{\langle ij}\frac{\partial \ln\rho}{\partial x_{k\rangle}} + \frac{4}{5}q_{\langle i}\frac{\partial v_j}{\partial x_{k\rangle}}\right), \tag{8}$$

with $S_{jk} = \partial v_{\langle j}/\partial x_{k\rangle}$.

In the continuum regime, where the Knudsen number is small, Eqs. (4) and (5) respectively reduce to Fourier and Navier–Stokes laws

$$q_i^{(\mathrm{NSF})} = -\frac{5}{2}\frac{\mu}{Pr}\frac{\partial\theta}{\partial x_i}, \qquad \sigma_{ij}^{(\mathrm{NSF})} = -2\mu\frac{\partial v_{\langle i}}{\partial x_{j\rangle}}, \tag{9}$$

where $\kappa = -5\mu/(2\,Pr)$ is the thermal conductivity coefficient for ideal gases. Comparing Eqs. (4) and (5) with Eq. (9) shows that in the hydrodynamic regime only the underlined terms stay within (4) and (5).

We emphasize that solutions for Eqs. (1)–(8) with $Pr = 2/3$ must be compared only to those kinetic data which are obtained based on the linearized Boltzmann kinetic model (LB). Comparison with the BGK data requires $Pr = 1$ in Eq. (4) and different coefficients in Eqs. (6)–(8). See the textbook [16, pg. 138] for the BGK coefficients.

Here we proceed with the presented form of the R13 equations and assume $Pr = 2/3$. At the end we validate our results with the linearized Boltzmann kinetic data.

3. Boundary conditions for regularized 13-moment equations for micro-channel flows

Construction of boundary conditions for extended continuum models is known as the most challenging task, when these models are considered for practical applications. Successful simulations with these extended equations strongly depends on both physical and mathematical consistencies between the boundary conditions and the equations.

Lowest-order moments which construct the classical NSF system and its corresponding boundary conditions all have meaningful physical interpretations, and can be measured on the boundary. However, in the Grad-type equations, there are no such physical interpretations for higher-order moments.

In theory, boundary conditions for high-order moments are available if details of gas–surface interaction are known. In the absence of such information, a simple argument going back to Maxwell can be utilized to derive required boundary conditions for the high-order moments. Accordingly, kinetic boundary conditions for the R13 equations [34,35] which are obtained from Maxwell's boundary condition for the Boltzmann equation (diffuse-reflection boundary condition) are used to solve the considered boundary value problem.

The full set of R13 kinetic boundary conditions for flows in planar geometry are [34]

$$\sigma_{12} = \frac{-\chi}{2-\chi}\sqrt{\frac{2}{\pi\theta}}\left(\mathcal{P}\mathcal{V}_1 + \frac{1}{5}q_1 + \frac{1}{2}m_{122}\right)n_2, \tag{10a}$$

$$q_2 = \frac{-\chi}{2-\chi}\sqrt{\frac{2}{\pi\theta}}\left(2\mathcal{P}\mathcal{T} - \frac{1}{2}\mathcal{P}\mathcal{V}^2 + \frac{1}{2}\theta\sigma_{22} + \frac{1}{15}\Delta + \frac{5}{28}R_{22}\right)n_2, \tag{10b}$$

$$R_{12} = \frac{\chi}{2-\chi}\sqrt{\frac{2}{\pi\theta}}\left(\mathcal{P}\theta\mathcal{V}_1 - \mathcal{P}\mathcal{V}_1^3 + 6\mathcal{P}\mathcal{T}\mathcal{V}_1 - \frac{11}{5}\theta q_1 - \frac{1}{2}\theta m_{122}\right)n_2, \tag{10c}$$

$$m_{222} = \frac{\chi}{2-\chi}\sqrt{\frac{2}{\pi\theta}}\left(\frac{2}{5}\mathcal{P}\mathcal{T} - \frac{3}{5}\mathcal{P}\mathcal{V}^2 - \frac{7}{5}\theta\sigma_{22} + \frac{1}{75}\Delta - \frac{1}{14}R_{22}\right)n_2, \tag{10d}$$

$$m_{112} = \frac{-\chi}{2-\chi}\sqrt{\frac{2}{\pi\theta}}\left(\frac{1}{14}R_{11} + \theta\sigma_{11} - \frac{1}{5}\theta\sigma_{22} - \frac{4}{5}\mathcal{P}\mathcal{V}^2 + \frac{1}{5}\mathcal{P}\mathcal{T} + \frac{1}{150}\Delta\right)n_2, \tag{10e}$$

with the abbreviations

$$\mathcal{P} = p + \frac{1}{2}\sigma_{22} - \frac{1}{120}\frac{\Delta}{\theta} - \frac{1}{28}\frac{R_{22}}{\theta}, \qquad \mathcal{V}_1 = v_1 - v_1^W, \qquad \mathcal{T} = \theta - \theta_W. \tag{11}$$

Velocity slip and temperature jump on the wall are presented by $\mathcal{V}_1 = v_1 - v_1^W$ and $\mathcal{T} = \theta - \theta_W$, respectively, with v_1^W and θ_W as wall velocity and temperature. The surface accommodation factor is denoted by χ, and for simplicity, we set $\chi = 1$, that is we consider fully diffusive boundaries. The wall normal vector is $\mathbf{n} = \{0, 1, 0\}$, where $n_2 = 1$ and $n_2 = -1$ represent normals of the lower and upper walls, respectively [cf. Fig. 1].

The requirement that mass is conserved in the process can be utilized as an auxiliary condition, i.e.,

$$\int_{-H/2}^{+H/2}\rho\mathrm{d}x_2 = \text{constant}, \tag{12}$$

which can be used to find the density distribution between the channel plates.

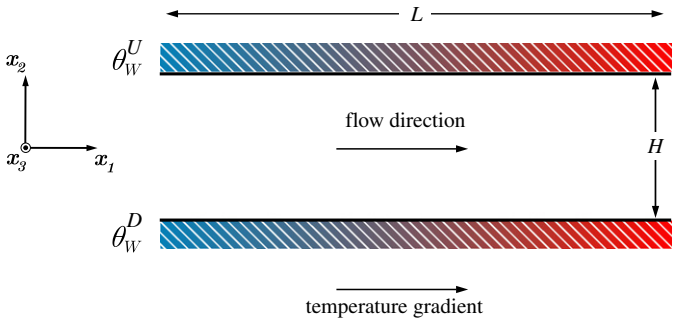

Fig. 1. Flow setting in thermal transpiration flow between two infinite parallel plates. Constant pressure flow is assumed $\partial p/\partial x_1 = 0$, and temperature gradient is considered to be positive in x_1-direction. Wall temperatures are θ_W^U and θ_W^D, which are symmetric around the centerline, $x_2 = 0$.

4. Problem statement

We consider the problem of steady state flow of a dilute ideal gas in a parallel-plate micro-channel, see Fig. 1. The infinite plates are parallel in direction x_1, separated by a distance H, located on $x_2 = \pm H/2$. Flow is independent of direction x_3, that is we consider rectangular channels with a large cross-sectional aspect ratio. A constant pressure flow is superimposed within the channel, $\partial_{x_1} p = 0$. The channel walls are stationary, impermeable and heated such that a constant temperature gradient, $\partial_{x_1}\theta_W = A$, exists in the walls. The body force is zero, $G_i = \{0, 0, 0\}$, and flow is driven as the result of the temperature gradient along the channel. Owing to the compressibility effects, we should consider a two-dimensional velocity vector [36], $v_i = \{v_1(x_1, x_2), v_2(x_1, x_2), 0\}$. Since the system is independent of direction x_3, heat-flux vector and symmetric trace-free stress tensor reduce to

$$q_i = \{q_1(x_1, x_2), q_2(x_1, x_2), 0\}\,, \tag{13}$$

and

$$\sigma_{ij} = \begin{Bmatrix} \sigma_{11}(x_1, x_2) & \sigma_{12}(x_1, x_2) & 0 \\ \sigma_{12}(x_1, x_2) & \sigma_{22}(x_1, x_2) & 0 \\ 0 & 0 & -\sigma_{11}(x_1, x_2) - \sigma_{22}(x_1, x_2) \end{Bmatrix}. \tag{14}$$

Nevertheless, it is important to emphasize that in the present work we do not attempt to tackle the two-dimensional problem, which demands a numerical solution. Instead, we consider any arbitrary cross-section along the channel and its corresponding local equilibrium condition to analytically express the local rarefaction effects. This is achieved by employing both linearized and semi-linearized R13 equations.

5. Linear approach

The temperature distribution in the walls is $\theta_W = \theta_0 + Ax_1$, where θ_0 is the wall temperature at reference location, $x_1^0 = 0$. For a sufficiently long channel the same temperature gradient exists in the flow. A corresponding reference equilibrium state (at the reference location, $x_1^0 = 0$) is defined by $\{\rho_0, \theta_0, v_i^0\}$, which is used for nondimensionalization and linearization. In fact, the reference temperature is set to the local wall temperature, and we are interested in the local difference between gas and wall temperatures. The reference density, ρ_0, relates the reference wall temperature to the pressure via the ideal gas law.

Dimensionless position vectors are $\tilde{x}_1 = x_1/L$ and $\tilde{x}_2 = x_2/H$, where H (height) and L (length) are macroscopic length scales; for a long micro-channel $\epsilon = H/L \ll 1$. Dimensionless density and temperature are defined as their deviation from the equilibrium state, $\tilde{\rho} = \rho/\rho_0 - 1$, and $\tilde{\theta} = \theta/\theta_0 - 1$. In the reference state, the moments assume the values $\rho_0 = \theta_0 = p_0 = 1$, and $v_i^0 = q_i^0 = \sigma_{ij}^0 = \Delta_0 = R_{ij}^0 = m_{ijk}^0 = 0$. The rest of the variables in dimensionless form read

$$\begin{aligned} \tilde{v}_i &= \frac{v_i}{\sqrt{\theta_0}}, & \tilde{\sigma}_{ij} &= \frac{\sigma_{ij}}{\rho_0\theta_0}, & \tilde{q}_i &= \frac{q_i}{\rho_0\sqrt{\theta_0}^3}, \\ \tilde{\Delta} &= \frac{\Delta}{\rho_0\theta_0^2}, & \tilde{R}_{ij} &= \frac{R_{ij}}{\rho_0\theta_0^2}, & \tilde{m}_{ijk} &= \frac{m_{ijk}}{\rho_0\sqrt{\theta_0}^3}, \end{aligned} \tag{15}$$

where $\sqrt{\theta_0}$ denotes thermal speed at the reference state. Also, $\tilde{\mu} = \mu/\mu_0 - 1$ is the dimensionless viscosity with $\mu_0 = \mu(\theta_0)$ as the reference viscosity. Accordingly, deviations vanish in the reference equilibrium state, i.e., $\tilde{\rho}_0 = \tilde{\theta}_0 = \tilde{\mu}_0 = 0$.

5.1. Linearized R13 equations

For the linearized equations, only terms that are linear in deviations from the reference equilibrium state are considered. This means that only very small temperature and density gradients are allowed, which implies $A \ll 1$. Accordingly, $\tilde{p} = 1 + \tilde{\rho} + \tilde{\theta}$ is the linearized equation of state for the ideal gas. The dimensionless and linearized continuity equation reads as

$$\epsilon \frac{\partial \tilde{v}_1}{\partial \tilde{x}_1} + \frac{\partial \tilde{v}_2}{\partial \tilde{x}_2} = 0, \tag{16}$$

which somehow represents an incompressible flow. The first terms is multiplied with the smallness parameter ϵ, and is negligible. In our fully linear approach, we claim that $\tilde{v}_2$ is a nonlinear effect. Consequently, we set $\tilde{v}_2 = 0$ in the following linear calculations, and finally, based on the obtained results, we will show that this assumption is consistent. Note that, according to this assumption, streamwise gradients of heat flux and stress vanish in the linear system.

In dimensionless variables, the R13 system [cf. Eqs. (1)–(8)] for the considered flow configuration reduce to the following ordinary differential systems.

(i) Velocity problem,

$$\frac{\mathrm{d}\tilde{\sigma}_{12}}{\mathrm{d}\tilde{x}_2} = 0, \tag{17a}$$

$$\frac{2}{5}\frac{\mathrm{d}\tilde{q}_1}{\mathrm{d}\tilde{x}_2} + \frac{\mathrm{d}\tilde{v}_1}{\mathrm{d}\tilde{x}_2} = -\frac{1}{Kn}\tilde{\sigma}_{12}, \tag{17b}$$

$$\frac{5}{2}\epsilon\frac{\mathrm{d}\tilde{\theta}}{\mathrm{d}\tilde{x}_1} - \frac{6}{5}Kn\frac{\mathrm{d}^2\tilde{q}_1}{\mathrm{d}\tilde{x}_2^2} = -\frac{2}{3Kn}\tilde{q}_1. \tag{17c}$$

(ii) Temperature problem,

$$\frac{\mathrm{d}\tilde{q}_2}{\mathrm{d}\tilde{x}_2} = 0, \tag{18a}$$

$$-\frac{6}{5}Kn\frac{\mathrm{d}^2\tilde{\sigma}_{22}}{\mathrm{d}\tilde{x}_2^2} = -\frac{1}{Kn}\tilde{\sigma}_{22}, \tag{18b}$$

$$\frac{5}{2}\frac{\mathrm{d}\tilde{\theta}}{\mathrm{d}\tilde{x}_2} + \frac{\mathrm{d}\tilde{\sigma}_{22}}{\mathrm{d}\tilde{x}_2} = -\frac{2}{3Kn}\tilde{q}_2. \tag{18c}$$

(iii) Density/pressure problem,

$$-\frac{2}{3}Kn\frac{\mathrm{d}^2\tilde{\sigma}_{11}}{\mathrm{d}\tilde{x}_2^2} + \frac{4}{15}Kn\frac{\mathrm{d}^2\tilde{\sigma}_{22}}{\mathrm{d}\tilde{x}_2^2} = -\frac{1}{Kn}\tilde{\sigma}_{11}, \tag{19a}$$

$$\frac{\mathrm{d}\tilde{\theta}}{\mathrm{d}\tilde{x}_2} + \frac{\mathrm{d}\tilde{\rho}}{\mathrm{d}\tilde{x}_2} + \frac{\mathrm{d}\tilde{\sigma}_{22}}{\mathrm{d}\tilde{x}_2} = 0. \tag{19b}$$

Here, $Kn = \lambda_0/H$ is the Knudsen number at the reference equilibrium state, with $\lambda_0 = \mu_0\sqrt{\theta_0}/p_0$ as the reference mean free path, i.e.,

$$Kn = \frac{\mu_0\sqrt{\theta_0}}{p_0 H}. \tag{20}$$

Eqs. (17a) and (19b) are momentum conservation laws in x_1 and x_2 directions, respectively, while Eq. (18a) is the linearized energy balance. The remaining equations are the extended balance equations for heat flux and stress. The term $\epsilon\ (\mathrm{d}\tilde{\theta}/\mathrm{d}\tilde{x}_1)$ in Eq. (17c) represents the dimensionless temperature gradient, $\alpha = AH/\theta_0$.

Integration of the above equations gives the general solution (C_1 to C_{11} are integrating constants)

$$\tilde{\sigma}_{12} = \mathsf{C}_1, \tag{21a}$$

$$\tilde{q}_1 = -\frac{15Kn\,\alpha}{4} + \mathsf{C}_2\sinh\left(\frac{\sqrt{5}}{3Kn}\tilde{x}_2\right) + \mathsf{C}_3\cosh\left(\frac{\sqrt{5}}{3Kn}\tilde{x}_2\right), \tag{21b}$$

$$\tilde{v}_1 = \mathsf{C}_4 - \frac{1}{Kn}\tilde{\sigma}_{12}\tilde{x}_2 - \frac{2}{5}\tilde{q}_1, \tag{21c}$$

and

$$\tilde{q}_2 = \mathsf{C}_5, \tag{22a}$$

$$\tilde{\sigma}_{22} = \mathsf{C}_6 \sinh\left(\frac{\sqrt{5}}{\sqrt{6}Kn}\tilde{x}_2\right) + \mathsf{C}_7 \cosh\left(\frac{\sqrt{5}}{\sqrt{6}Kn}\tilde{x}_2\right), \tag{22b}$$

$$\tilde{\theta} = \mathsf{C}_8 - \frac{4}{15Kn}\tilde{q}_2\,\tilde{x}_2 - \frac{2}{5}\tilde{\sigma}_{22}, \tag{22c}$$

and finally for the density/pressure problem

$$\tilde{\sigma}_{11} = \mathsf{C}_9 \sinh\left(\frac{\sqrt{3}}{\sqrt{2}Kn}\tilde{x}_2\right) + \mathsf{C}_{10} \cosh\left(\frac{\sqrt{3}}{\sqrt{2}Kn}\tilde{x}_2\right) - \frac{1}{2}\tilde{\sigma}_{22}, \tag{23a}$$

$$\tilde{\rho} = \mathsf{C}_{11} - \tilde{\theta} - \tilde{\sigma}_{22}. \tag{23b}$$

The hyperbolic functions in Eqs. (21b), (22b) and (23a) describe Knudsen boundary layers, which are absent in hydrodynamic (Navier–Stokes–Fourier) solution. Note that σ_{11} and σ_{22} are pure Knudsen boundary layers, and thus are pure rarefaction effects. The solutions for the other macroscopic quantities are superpositions of bulk solutions and Knudsen layers, e.g., solution for $\tilde{q}_1$ is summation of Knudsen layers (hyperbolic sine and cosine terms) and bulk solution, $\tilde{q}_1^{\mathrm{NSF}} = -15Kn\,\alpha/4$.

5.2. Linearized boundary conditions

Boundary conditions are required to evaluate integrating constants in our solutions [cf. Eqs. (21)–(23)]. To be consistent with the linearized equations, we should use linear boundary conditions as well. The kinetic boundary conditions [cf. Eq. (10)] in their dimensionless and linear form read

$$\tilde{\sigma}_{12} = \frac{-\chi}{2-\chi}\sqrt{\frac{2}{\pi}}\left(\tilde{\mathcal{V}}_1 + \frac{1}{5}\tilde{q}_1 + \frac{1}{2}\tilde{m}_{122}\right) n_2, \tag{24a}$$

$$\tilde{q}_2 = \frac{-\chi}{2-\chi}\sqrt{\frac{2}{\pi}}\left(2\tilde{\mathcal{T}} + \frac{1}{2}\tilde{\sigma}_{22} + \frac{1}{15}\tilde{\Delta} + \frac{5}{28}\tilde{R}_{22}\right) n_2, \tag{24b}$$

$$\tilde{R}_{12} = \frac{\chi}{2-\chi}\sqrt{\frac{2}{\pi}}\left(\tilde{\mathcal{V}}_1 - \frac{11}{5}\tilde{q}_1 - \frac{1}{2}\tilde{m}_{122}\right) n_2, \tag{24c}$$

$$\tilde{m}_{222} = \frac{\chi}{2-\chi}\sqrt{\frac{2}{\pi}}\left(\frac{2}{5}\tilde{\mathcal{T}} - \frac{7}{5}\tilde{\sigma}_{22} + \frac{1}{75}\tilde{\Delta} - \frac{1}{14}\tilde{R}_{22}\right) n_2, \tag{24d}$$

$$\tilde{m}_{112} = \frac{-\chi}{2-\chi}\sqrt{\frac{2}{\pi}}\left(\frac{1}{14}\tilde{R}_{11} + \tilde{\sigma}_{11} - \frac{1}{5}\tilde{\sigma}_{22} + \frac{1}{5}\tilde{\mathcal{T}} + \frac{1}{150}\tilde{\Delta}\right) n_2. \tag{24e}$$

Due to the symmetry of flow with respect to the center line ($\tilde{x}_2 = 0$), terms that are odd functions of $\tilde{x}_2$ will vanish in the solutions, so that

$$\mathsf{C}_1 = \mathsf{C}_2 = \mathsf{C}_5 = \mathsf{C}_6 = \mathsf{C}_9 = 0. \tag{25}$$

The remaining integrating constants will be determined from the above boundary conditions at the lower wall, where the normal vector of the boundary is $\mathbf{n} = \{0, 1, 0\}$, see Fig. 1. Thus, five boundary conditions will suffice to find $\{\mathsf{C}_3, \mathsf{C}_4, \mathsf{C}_7, \mathsf{C}_8, \mathsf{C}_{10}\}$.

The constant C_{11} follows from Eq. (12), which assumes the form

$$\int_{-1/2}^{+1/2} \rho/\rho_0 \mathrm{d}\tilde{x}_2 = \int_{-1/2}^{+1/2} (\tilde{\rho} + 1)\,\mathrm{d}\tilde{x}_2 = 1. \tag{26}$$

5.3. Linear results

For the linear case, with the help of fully linear boundary conditions, the unknown integrating constants are found as

$$\mathsf{C}_3 = \alpha Kn \frac{\frac{45\chi}{2-\chi}\sqrt{\frac{2}{\pi}}}{\frac{12\chi}{2-\chi}\sqrt{\frac{2}{\pi}}\cosh\left(\frac{\sqrt{5}}{6Kn}\right) + 4\sqrt{5}\sinh\left(\frac{\sqrt{5}}{6Kn}\right)}, \tag{27a}$$

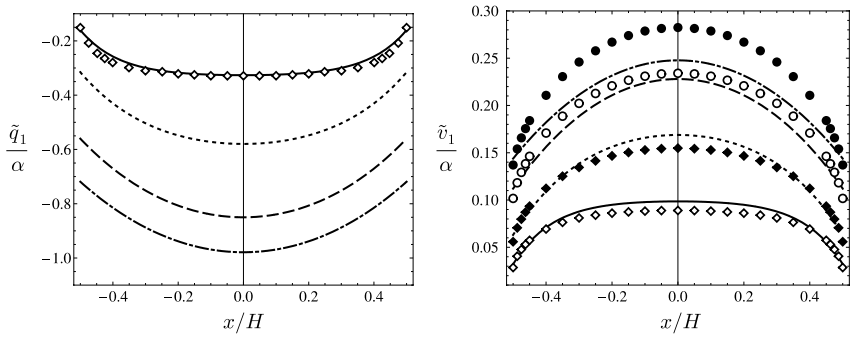

Fig. 2. Dimensionless distribution of normalized heat flux $\tilde{q}_1/\alpha$ and velocity $\tilde{v}_1/\alpha$ across the channel are show for transpiration flow. The R13 results (lines) which are obtained for fully diffusive walls $\chi = 1$ in different Knudsen numbers are compared to kinetic data (symbols) from Ref. [14]. For the sake of consistency in comparison, the dimensionless kinetic data are multiplied with $\sqrt{2}$. (Solid line, white diamonds) $Kn = 0.088$; (dotted line, black diamonds) $Kn = 0.177$; (dashed line, white circles) $Kn = 0.353$; (dash-dotted line, black circles) $Kn = 0.530$.

$$\mathsf{C}_4 = \alpha Kn \frac{-3\sqrt{5}\sinh\left(\frac{\sqrt{5}}{6Kn}\right)}{\frac{12\chi}{2-\chi}\sqrt{\frac{2}{\pi}}\cosh\left(\frac{\sqrt{5}}{6Kn}\right) + 4\sqrt{5}\sinh\left(\frac{\sqrt{5}}{6Kn}\right)}, \tag{27b}$$

$$\mathsf{C}_7 = \mathsf{C}_8 = \mathsf{C}_{10} = \mathsf{C}_{11} = 0, \tag{27c}$$

which must be used in the linear solutions [cf. Eqs. (21)–(23)]. Accordingly, the local solution for the linear problem reads

$$\tilde{\sigma}_{11} = \tilde{\sigma}_{12} = \tilde{\sigma}_{22} = \tilde{q}_2 = \tilde{\theta} = \tilde{\rho} = 0, \tag{28a}$$

$$\tilde{q}_1 = -\frac{15Kn\,\alpha}{4} + \mathsf{C}_3 \cosh\left(\frac{\sqrt{5}}{3Kn}\tilde{x}_2\right), \tag{28b}$$

$$\tilde{v}_1 = \mathsf{C}_4 + \frac{3Kn\,\alpha}{2} - \frac{2\mathsf{C}_3}{5}\cosh\left(\frac{\sqrt{5}}{3Kn}\tilde{x}_2\right), \tag{28c}$$

where $\mathsf{C}_4 + 3Kn\,\alpha/2$ in Eq. (28c) represent the slip velocity (temperature-driven plug flow). The solution in (28) shows that in the linear limit nonequilibrium effects arise only for the tangential heat flux and velocity, while the other quantities remain in the local reference state.

Conventionally, in kinetic approaches a rarefaction parameter k for channel flows is defined as

$$k = \frac{\sqrt{\pi}}{2}\frac{H}{\lambda_0}, \tag{29}$$

where H and λ are reference length scale (height of the channel) and mean free path, respectively. The kinetic theory of gases gives the mean free path with respect to macroscopic quantities, i.e.,

$$\lambda_0 = \sqrt{\frac{\pi\theta_0}{2}}\frac{\mu_0}{p_0}. \tag{30}$$

Replacement of λ from Eq. (30) into Eq. (29) and then comparison with Eq. (20) gives

$$Kn = \frac{1}{\sqrt{2}k}, \tag{31}$$

which relates our definition of the Knudsen number to that which is used in kinetic approaches.

Profiles for normalized velocity and parallel heat flux, according to Eqs. (28b) and (28c) are depicted in Fig. 2. These results are compared with direct numerical solutions of the linear Boltzmann equation from Ref. [14]. The plots are shown for four different Knudsen numbers and perfectly diffusive walls, $\chi = 1$. As postulated by the Fourier's law, the tangential heat flow is in the opposite direction of the temperature gradient; from hot to cold. The decrease of heat flow close to the walls is due to the non-Fourier contribution in the Knudsen layer, i.e., the hyperbolic cosine function in Eq. (28b). Unlike the thermal energy flow, the velocity plots show that mass flow is in the direction of the temperature gradient. The slip velocity on the walls are predicted with an outstanding accuracy. This gives further evidence of the reliability of the applied boundary conditions. As expected, the R13 system is reliable within the transition regime ($Kn \leqslant 0.5$), hence for $k = 0.6$ (or $Kn = 0.53$) some deviations from the Boltzmann solution appear in the bulk flow.

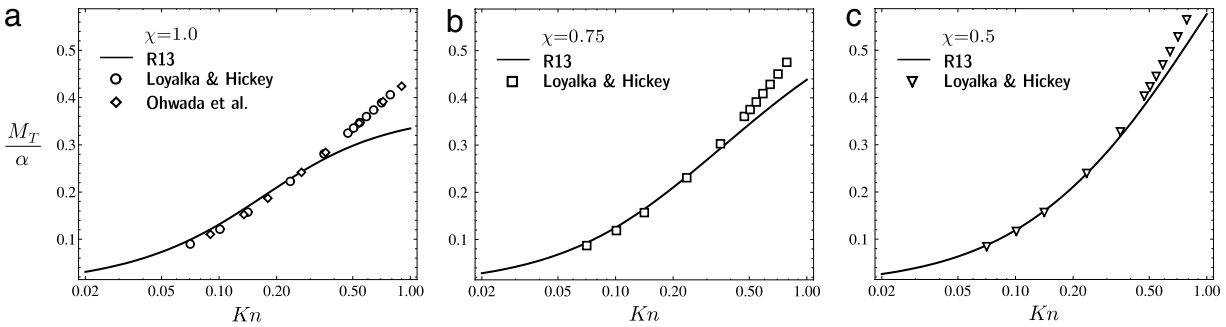

Fig. 3. The normalized mass flow rate M_T/α vs. Kn in thermal transpiration flow. The R13 results (solid line) are compared to linearized Boltzmann data (symbols) from Refs. [14,15]. Dependence of mass flow rate on accommodation coefficient χ are shown in the plots. In transpiration flow, mass flow rate diverges infinitely in the limit of free molecular flow when $Kn \to \infty$, and vanishes in the continuum limit, i.e., $Kn \to 0$.

While in the force-driven Poiseuille flow mass flux vs. Knudsen number exhibits the so-called Knudsen minimum, in the temperature-driven flow, mass flux increases with Knudsen number. We define the mass flow rate M_T as [8,14,15]

$$M_T = \sqrt{2}\int_{-1/2}^{+1/2} \tilde{v}_1 \mathrm{d}\tilde{x}_2, \tag{32}$$

where the required velocity function is given in Eq. (28c), and the factor $\sqrt{2}$ is used for consistency with the kinetic data. This integral yields a linear expression in α for the mass flow rate,

$$M_T = \alpha \frac{3Kn}{2\sqrt{2}} \left(2 - \frac{5\sqrt{\pi} + \frac{36\sqrt{2}\chi}{2-\chi} Kn}{5\sqrt{\pi} + \frac{3\sqrt{10}\chi}{2-\chi} \coth\left(\frac{\sqrt{5}}{6Kn}\right)} \right). \tag{33}$$

In Fig. 3, our results for the normalized mass flow rate M_T/α are compared with kinetic data from Refs. [14,15] which are the solutions for the linearized Boltzmann equation. In the plots, mass flow rates for different surface accommodation coefficients $\chi = \{1.0, 0.75, 0.5\}$ are compared. As illustrated, for larger Knudsen numbers, smooth channels with small accommodation coefficients allow larger mass flow rates. This occurs due to the slip increase on the channel walls. For fully diffuse walls ($\chi = 1$) our results agree with kinetic data for $Kn < 0.5$ [cf. plot (a)], while for $\chi = 0.5$ the R13 results are valid for $Kn < 0.7$, see plot (c). As shown previously for Couette and Poiseuille flows [27,28,34,37], the validity of R13 equations within the transition regime is again confirmed here.

Similar to the mass flow rate, the thermal energy flow rate E_T can be defined as [8,15]

$$E_T = -\sqrt{2}\int_{-1/2}^{+1/2} \tilde{q}_1 \mathrm{d}\tilde{x}_2, \tag{34}$$

where the required heat flux function is given in Eq. (28b). This integral yields a linear expression in α for the thermal energy flow rate,

$$E_T = \alpha \frac{3Kn}{2\sqrt{2}} \left(5 - \frac{\frac{36\sqrt{5}\chi}{2-\chi} Kn}{\sqrt{10\pi} + \frac{6\chi}{2-\chi} \coth\left(\frac{\sqrt{5}}{6Kn}\right)} \right), \tag{35}$$

which similar to M_T is a function of dimensionless temperature gradient α, surface accommodation coefficient χ, and Knudsen number Kn.

In Fig. 4, we compare our results for the normalized thermal energy flow rate E_T/α with the kinetic data in Ref. [15]. Variations of energy flow rate with respect to χ and Kn is similar to the mass flow rate.

5.4. Consistency of linear results

The nonvanishing constants in Eq. (27) are all first-order in α, thus, as shown in Eq. (28), $\mathcal{O}\left(\tilde{q}_1\right) = \mathcal{O}\left(\tilde{v}_1\right) = \mathcal{O}\left(\mathrm{d}\tilde{v}_1/\mathrm{d}\tilde{x}_2\right) = \mathcal{O}\left(\mathrm{d}\tilde{q}_1/\mathrm{d}\tilde{x}_2\right) = \mathcal{O}\left(\alpha\right)$. Those nonequilibrium quantities that vanish in the linear limit, i.e., $\left\{\tilde{\sigma}_{11}, \tilde{\sigma}_{12}, \tilde{\sigma}_{22}, \tilde{q}_2\right\}$, should be second-order (or higher) in α.

Recall that in our linear approach, in order to simplify the continuity equation, we assumed $v_2 = 0$. Now, this assumption can be justified using the linear results. The steady state continuity equation can be written as

$$\rho\frac{\partial v_1}{\partial x_1} + v_1\frac{\partial \rho}{\partial x_1} + \frac{\partial \rho v_2}{\partial x_2} = 0, \tag{36}$$

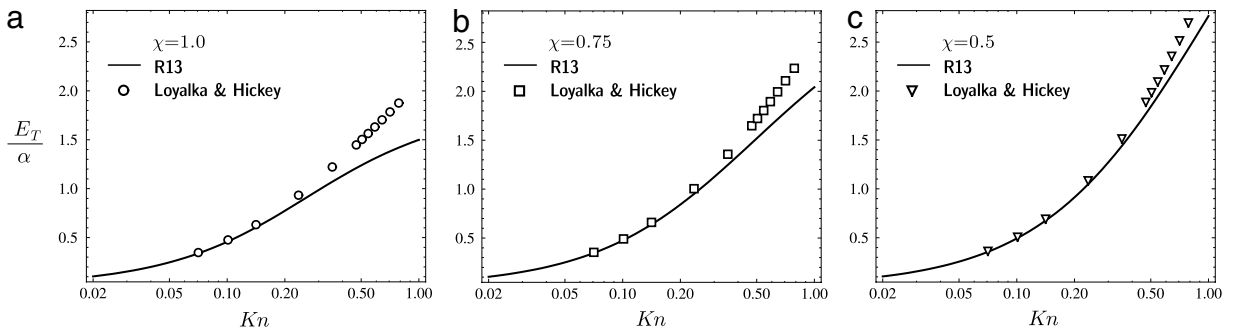

Fig. 4. The normalized thermal energy flow rate E_T/α vs. Kn in thermal transpiration flow. The R13 results (solid line) are compared to linearized Boltzmann data (symbols) from Ref. [15]. Dependence of thermal energy flow rate on accommodation coefficient χ are shown in the plots. In transpiration flow, energy flow rate diverges infinitely in the limit of free molecular flow when $Kn \to \infty$, and vanishes in the continuum limit, i.e., $Kn \to 0$.

where, according to the linear solution, the first term is zero and the second one is of the order α^2, since $\partial_{\tilde{x}_1}\tilde{\theta} = -\partial_{\tilde{x}_1}\tilde{\rho} = \alpha$. Therefore, the last term should be second order in α, and is zero in the linear case. This argument gives $\rho v_2 = \text{const}$, which is valid within the linear theory. Finally, the boundary condition of impermeable walls requires that $v_2 = 0$.

6. Semi-linear approach

In the semi-linear approach we include some nonlinear terms within the R13 equations which are of order α^2. Referring to the linear results, $\tilde{q}_1(\mathrm{d}\tilde{v}_1/\mathrm{d}\tilde{x}_2)$ (and its derivative with respect to $\tilde{x}_2$) is the only nonlinear term in the R13 equations that is certainly of second-order in α.

In the semi-linear case, unlike the linear one, we cannot assure a one-dimensional flow. However, in order to decouple, and analytically solve the equations, we assume $\tilde{v}_2 = 0$. Under the assumption of one-dimensional flow the continuity equation reduces to $\tilde{v}_1\partial_{\tilde{x}_1}\tilde{\rho} + \partial_{\tilde{x}_1}\tilde{v}_1 = 0$, which describes the compressibility effects along the channel. In the present study, we are not interested in the two-dimensional problem of compressible flow along the channel, instead, we focus on local solution, that is profiles across the channel.

Moreover, we consider sufficiently long micro-channels where $\mathcal{O}(\epsilon) = \mathcal{O}(\alpha)$. This dimensional assumption leads to neglection of streamwise flow deviations, as they appear to be of third-order (or higher) in α.

6.1. Semi-linearized R13 equations

To study the coupling between tangential heat flux and velocity gradient (shear rate) we introduce $\tilde{q}_1(\mathrm{d}\tilde{v}_1/\mathrm{d}\tilde{x}_2)$, and its derivative with respect to $\tilde{x}_2$ into the linear R13 equations.

Incorporation of these nonlinear terms does not affect the linear velocity problem, however, the semi-linearized temperature problem now becomes

$$\frac{\mathrm{d}\tilde{q}_2}{\mathrm{d}\tilde{x}_2} = 0, \tag{37a}$$

$$-\frac{6}{5}Kn\frac{\mathrm{d}^2\tilde{\sigma}_{22}}{\mathrm{d}\tilde{x}_2^2} + \underline{\frac{8}{25}Kn\frac{\mathrm{d}}{\mathrm{d}\tilde{x}_2}\left(\tilde{q}_1\frac{\mathrm{d}\tilde{v}_1}{\mathrm{d}\tilde{x}_2}\right)} = -\frac{1}{Kn}\tilde{\sigma}_{22}, \tag{37b}$$

$$\frac{5}{2}\frac{\mathrm{d}\tilde{\theta}}{\mathrm{d}\tilde{x}_2} + \frac{\mathrm{d}\tilde{\sigma}_{22}}{\mathrm{d}\tilde{x}_2} + \underline{\frac{2}{5}\tilde{q}_1\frac{\mathrm{d}\tilde{v}_1}{\mathrm{d}\tilde{x}_2}} = -\frac{2}{3Kn}\tilde{q}_2, \tag{37c}$$

and the semi-linearized density/pressure problem becomes

$$-\frac{2}{3}Kn\frac{\mathrm{d}^2\tilde{\sigma}_{11}}{\mathrm{d}\tilde{x}_2^2} + \frac{4}{15}Kn\frac{\mathrm{d}^2\tilde{\sigma}_{22}}{\mathrm{d}\tilde{x}_2^2} - \underline{\frac{32}{75}Kn\frac{\mathrm{d}}{\mathrm{d}\tilde{x}_2}\left(\tilde{q}_1\frac{\mathrm{d}\tilde{v}_1}{\mathrm{d}\tilde{x}_2}\right)} = -\frac{1}{Kn}\tilde{\sigma}_{11}, \tag{38a}$$

$$\frac{\mathrm{d}\tilde{\rho}}{\mathrm{d}\tilde{x}_2} + \frac{\mathrm{d}\tilde{\theta}}{\mathrm{d}\tilde{x}_2} + \frac{\mathrm{d}\tilde{\sigma}_{22}}{\mathrm{d}\tilde{x}_2} = 0. \tag{38b}$$

The underlined terms in Eqs. (37) and (38) correspond to the nonlinear terms. By employing the solutions of the linear velocity problem, and considering the symmetry with respect to the channel center [cf. Eq. (25)] the general solutions for

the above ODEs are obtained as

$$\tilde{q}_2 = 0, \tag{39a}$$

$$\tilde{\sigma}_{22} = \mathsf{C}_7 \cosh\left(\frac{\sqrt{5}}{\sqrt{6}Kn}\tilde{x}_2\right) - \frac{4\mathsf{C}_3 Kn\,\alpha}{5}\cosh\left(\frac{\sqrt{5}}{3Kn}\tilde{x}_2\right) - \frac{16\mathsf{C}_3^2}{375}\cosh\left(\frac{2\sqrt{5}}{3Kn}\tilde{x}_2\right), \tag{39b}$$

$$\tilde{\theta} = \mathsf{C}_8 - \frac{2\mathsf{C}_7}{5}\cosh\left(\frac{\sqrt{5}}{\sqrt{6}Kn}\tilde{x}_2\right) + \frac{2\mathsf{C}_3 Kn\,\alpha}{25}\cosh\left(\frac{\sqrt{5}}{3Kn}\tilde{x}_2\right) + \frac{62\mathsf{C}_3^2}{1875}\cosh\left(\frac{2\sqrt{5}}{3Kn}\tilde{x}_2\right), \tag{39c}$$

and

$$\tilde{\sigma}_{11} = -\frac{\mathsf{C}_7}{2}\cosh\left(\frac{\sqrt{5}}{\sqrt{6}Kn}\tilde{x}_2\right) + \frac{64\mathsf{C}_3 Kn\,\alpha}{85}\cosh\left(\frac{\sqrt{5}}{3Kn}\tilde{x}_2\right) + \frac{704\mathsf{C}_3^2}{4875}\cosh\left(\frac{2\sqrt{5}}{3Kn}\tilde{x}_2\right) + \mathsf{C}_{10}\cosh\left(\frac{\sqrt{3}}{\sqrt{2}Kn}\tilde{x}_2\right), \tag{40a}$$

$$\tilde{\rho} = \mathsf{C}_{11} - \tilde{\theta} - \tilde{\sigma}_{22}. \tag{40b}$$

Comparison of the above solutions with Eqs. (22) and (23) shows that the consequence of including the nonlinear terms is the formation of more Knudsen layers and additional bulk terms.

6.2. Semi-linearized boundary conditions

For semi-linear calculations, nonlinear behavior should be observed from the boundary conditions as well. In the boundary conditions for temperature and density problems [cf. Eqs. (10b), (10d) and (10e)], $\tilde{\mathcal{V}}_1^2$ is the only term that is second-order in α. Then, semi-linear boundary conditions to be used for determination of the unknown constants in Eqs. (39) and (40) are

$$\tilde{q}_2 = \frac{-\chi}{2-\chi}\sqrt{\frac{2}{\pi}}\left(2\tilde{\mathcal{T}} - \underline{\frac{1}{2}\tilde{\mathcal{V}}^2} + \frac{1}{2}\tilde{\sigma}_{22} + \frac{1}{15}\tilde{\Delta} + \frac{5}{28}\tilde{R}_{22}\right)n_2, \tag{41a}$$

$$\tilde{m}_{222} = \frac{\chi}{2-\chi}\sqrt{\frac{2}{\pi}}\left(\frac{2}{5}\tilde{\mathcal{T}} - \underline{\frac{3}{5}\tilde{\mathcal{V}}^2} - \frac{7}{5}\tilde{\sigma}_{22} + \frac{1}{75}\tilde{\Delta} - \frac{1}{14}\tilde{R}_{22}\right)n_2, \tag{41b}$$

$$\tilde{m}_{112} = \frac{-\chi}{2-\chi}\sqrt{\frac{2}{\pi}}\left(\frac{1}{5}\tilde{\mathcal{T}} - \underline{\frac{4}{5}\tilde{\mathcal{V}}^2} + \tilde{\sigma}_{11} - \frac{1}{5}\tilde{\sigma}_{22} + \frac{1}{150}\tilde{\Delta} + \frac{1}{14}\tilde{R}_{11}\right)n_2. \tag{41c}$$

The nonlinear terms are underlined.

6.3. Semi-linear results

For the semi-linearized system the velocity problem remains unchanged, i.e., C_3 and C_4 are the same as calculated for the linear case, see Eqs. (27a) and (27b). The constants $\{\mathsf{C}_7, \mathsf{C}_8, \mathsf{C}_{10}, \mathsf{C}_{11}\}$ turn out to be nonzero coefficients which are quadratic in α, however, their lengthly expressions are not presented here.

All terms in Eqs. (39) and (40) are second-order in α, which is why they did not appear in the fully linear solutions. Moreover, the above solutions are completely constructed by Knudsen layers (all terms include hyperbolic cosine functions), where C_8 is related to the temperature jump. To our knowledge, nonlinear effects in transpiration flow have not been investigated so far. Thus, we were unable to find any previously published data for comparison sake. Figure 5 shows the normalized distributions of temperature, density, and non-Newtonian stress components. As shown, when the flow becomes more rarefied, the Knudsen layers extend further into the bulk.

7. Conclusion

Fully linearized and semi-linearized forms of the regularized 13-moment equations were employed to investigate thermally-driven rarefied gas flows in parallel-plate micro-channels, where analytical solutions for both linearized and semi-linearized systems are accessible. In the linear case and for fully diffusive walls which are common in engineering applications, the accuracy of our results is confirmed with linear Boltzmann equation data up to a Knudsen number of around 0.5. All nonlinear terms in the semi-linearized equations correspond to the coupling between parallel heat flux and shear rate, which yields temperature, density, and non-Newtonian stress solutions as a superposition of several Knudsen layers.

The important advantage of the presented approach, as compared to numerical solutions of the Boltzmann equation, is its minimal computational effort. Also, an approximate macroscopic approach is presented to predict nonlinear effects. It seems that nonlinear effects in transpiration flow were not considered elsewhere. Although these effects are small, they should appear in solutions of the Boltzmann equation, either by direct numerical simulation, or by means of the direct simulation Monte Carlo (DSMC) method.

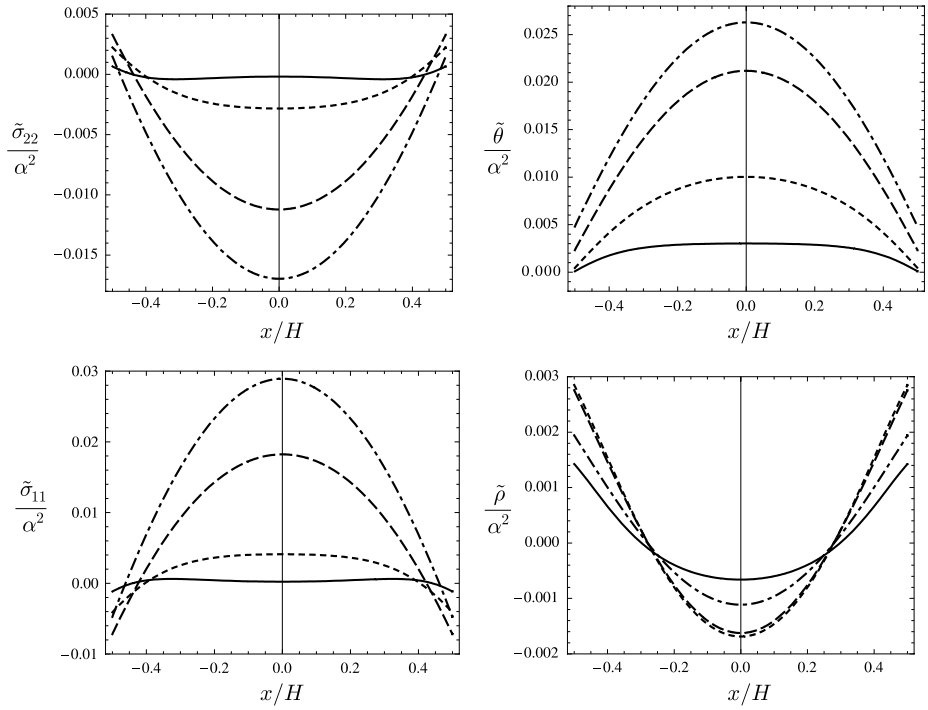

Fig. 5. Dimensionless distribution of normalized stress components $\{\tilde{\sigma}_{11}/\alpha^2, \tilde{\sigma}_{22}/\alpha^2\}$, temperature $\tilde{\theta}/\alpha^2$, and density $\tilde{\rho}/\alpha^2$ across the channel are show for transpiration flow. Semi-linearized R13 results which are obtained for fully diffusive walls $\chi = 1$ in different Knudsen numbers are shown. Note that in the linear theory all these quantities are constant, i.e., remain unchanged with respect to the reference equilibrium state. (Solid line) $Kn = 0.088$; (dotted line) $Kn = 0.177$; (dashed line) $Kn = 0.353$; (dash-dotted line) $Kn = 0.530$.

Acknowledgement

This research was supported by the Natural Sciences and Engineering Council (NSERC).

References

[1] Y. Sone, Kinetic Theory and Fluid Dynamics, Birkhäuser, Boston, 2002.
[2] O. Reynolds, Experimental researches on thermal transpiration of gases through porous plates and on the law of transpiration and impulsion, Philos. Trans. R. Soc. Lon. 170 (1879) 727.
[3] C. Maxwell, On stress in rarefied gases arising from inequalities of temperature, Philos. Trans. R. Soc. Lon. 170 (1879) 231.
[4] M. Knudsen, Eine Revision der Gleichgewichtsbedingung der Gase. Thermische Molekularströmung, Ann. Phys. 31 (1910) 205–229.
[5] M. Knudsen, Thermischer Molekulardruck der Gase in Röhren, Ann. Phys. 33 (1910) 1435.
[6] Y. Sone, Y. Waniguchi, K. Aoki, One-way flow of a rarefied gas induced in a channel with a periodic temperature distribution, Phys. Fluids 8 (1996) 227.
[7] Y.-L. Han, E.P. Muntz, A. Alexeenko, M. Young, Experimental and computational studies of temperature gradient-driven molecular transport in gas flows through nano/microscale channels, Nano. Microscale Thermophys. Eng. 11 (2007) 151.
[8] F. Sharipov, V. Seleznev, Data on internal rarefied gas flows, J. Phys. Chem. Ref. Data 27 (3) (1998) 657–706.
[9] S.K. Loyalka, Kinetic theory of thermal transpiration and mechanocaloric effect. i, J. Chem. Phys. 55 (9) (1971) 4497–4503.
[10] S.K. Loyalka, Comments on Poiseuille flow and thermal creep of a rarefied gas between parallel plates, Phys. Fluids 17 (1974) 1053.
[11] S.K. Loyalka, Kinetic theory of thermal transpiration and mechanocaloric effect. ii, J. Chem. Phys. 63 (9) (1975) 4054–4060.
[12] S.K. Loyalka, N. Petrellis, T.S. Storvick, Some exact numerical results for the BGK model: Couette, Poiseuille and thermal creep flow between parallel plates, J. Appl. Math. Phys. (ZAMP) 30 (1979) 514–521.
[13] L.B. Barichello, M. Camargo, P. Rodrigues, C.E. Siewert, Unified solutions to classical flow problems based on the BGK model, J. Appl. Math. Phys. (ZAMP) 52 (2001) 517–534.
[14] T. Ohwada, Y. Sone, K. Aoki, Numerical analysis of the Poiseuille and thermal transpiration flows between two parallel plates on the basis of the Boltzmann equation for hard-sphere molecules, Phys. Fluids A 1 (1989) 2042.
[15] S.K. Loyalka, K.A. Hickey, Kinetic theory of thermal transpiration and the mechanocaloric effect: planar flow of a rigid sphere gas with arbitrary accommodation at the surface, J. Vac. Sci. Technol. A 9 (1991) 158–163.
[16] H. Struchtrup, Macroscopic Transport Equations for Rarefied Gas Flows, Springer, New York, 2005.
[17] S. Chapman, T.G. Cowling, The Mathematical Theory of Nonuniform Gases, Cambridge University Press, Cambridge, 1970.
[18] H. Grad, On the kinetic theory of rarefied gases, Comm. Pure Appl. Math. 2 (1949) 325.
[19] H. Grad, in: S. Flügge (Ed.), Principles of the Kinetic Theory of Gases, in: Handbuch der Physik, vol. 12, Springer, Berlin, 1958.
[20] A.V. Bobylev, The Chapman–Enskog and grad methods for solving the Boltzmann equation, Sov. Phys. Dokl. 27 (1982) 29.
[21] P. Rosenau, Extending hydrodynamics via the regularization of the Chapman–Enskog expansion, Phys. Rev. A 40 (1989) 7193.
[22] X. Zhong, R.W. MacCormack, D.R. Chapman, Stabilization of the Burnett equations and applications to hypersonic flows, AIAA J. 31 (1993) 1036.
[23] S. Jin, M. Slemrod, Regularization of the Burnett equations via relaxation, J. Stat. Phys. 103 (2001) 1009.
[24] I. Müller, D. Reitebuch, W. Weiss, Extended thermodynamics — consistent in order of magnitude, Cont. Mech. Thermodyn. 15 (2003) 113.
[25] A.V. Bobylev, Instabilities in the Chapman–Enskog expansion and hyperbolic Burnett equations, J. Stat. Phys. 124 (2006) 371.

[26] L.H. Söderholm, Hybrid Burnett equations: a new method of stabilizing, Trans. Theory Stat. Phys. 36 (2007) 495.
[27] P. Taheri, M. Torrilhon, H. Struchtrup, Couette and Poiseuille microflows: analytical solutions for regularized 13-moment equations, Phys. Fluids 21 (2009) 017102.
[28] H. Struchtrup, M. Torrilhon, Higher-order effects in rarefied channel flows, Phys. Rev. E 78 (2008) 046301.
[29] P. Taheri, A.S. Rana, M. Torrilhon, H. Struchtrup, Macroscopic description of steady and unsteady rarefaction effects in boundary value problems of gas dynamics, Cont. Mech. Thermodyn. 21 (2009) 423–443.
[30] H. Struchtrup, Stable transport equations for rarefied gases at high orders in the knudsen number, Phys. Fluids 16 (2004) 3921.
[31] H. Struchtrup, M. Torrilhon, Regularization of grad's 13-moment equations: derivation and linear analysis, Phys. Fluids 15 (2003) 2668.
[32] H. Struchtrup, T. Thatcher, Bulk equations and Knudsen layers for the regularized 13 moment equations, Cont. Mech. Thermodyn. 19 (2007) 177.
[33] M. Torrilhon, H. Struchtrup, Regularized 13-moment equations: shock structure calculations and comparison to Burnett models, J. Fluid Mech. 513 (2004) 171.
[34] M. Torrilhon, H. Struchtrup, Boundary conditions for regularized 13-moment equations for micro-channel flows, J. Comput. Phys. 227 (2008) 1982.
[35] X. Gu, D. Emerson, A computational strategy for the regularized 13 moment equations with enhanced wall-boundary conditions, J. Comput. Phys. 225 (2007) 263.
[36] E.B. Arkilic, M.A. Schmidt, K.S. Breuer, Gaseous slip flow in long microchannels, J. Microelectromech. Syst. 6 (1997) 167.
[37] H. Struchtrup, M. Torrilhon, H theorem, regularization, and boundary conditions for linearized 13-moment equations, Phys. Rev. Lett. 99 (2007) 014502.